Research Square

Preprints are preliminary reports that have not undergone peer review.
They should not be considered conclusive, used to inform clinical practice,
or referenced by the media as validated information.

Heat stress induced gut microbiota changes activate TLR4 / NF-κB signaling pathway contributing to inflammatory bowel disease in pigs

Canying Hu
Guangdong Ocean University
Patil Yadnyavalkya
Lincoln University
Dongliang Gong
Guangdong Ocean University
Tianyue Yu
Guangdong Ocean University
Junyu Li
Guangdong Ocean University
Lianyun Wu
Guangdong Ocean University
Xiaoxi Liu
Guangdong Ocean University
Zhichao Yu
Guangdong Ocean University
Xinbing Ma
Guangdong Ocean University
Jinjun Chen
Guangdong Ocean University
Ravi Gooneratne
Lincoln University
Yanhong Yong
Guangdong Ocean University
Xianghong Ju (juxh77@163.com)
https://orcid.org/0000-0001-8822-484X

Research

Keywords:

Posted Date: January 22nd, 2020

DOI: https://doi.org/10.21203/rs.2.21626/v1

License: This work is licensed under a Creative Commons Attribution 4.0 International License.
Read Full License

Abstract

Background Various stressors alter the 'brain-gut axis' and contribute to many gastrointestinal disorders such as inflammatory bowel disease. However, the pathological mechanisms of these perturbations are poorly understood. Here, we report on the induction of intestinal inflammation in heat-stressed pigs and apply fecal microbiota transplantation from pigs to mice to elucidate the role of intestinal microbiota in TLR4/NF-κB signaling pathway activation. Results Twelve healthy adult pigs were subjected to heat stress (34 ± 1 °C and 75–85% relative humidity) and compared with 12 control pigs exposed to 25 ± 3 °C and the same humidity level. The pigs were sacrificed on days 1, 7, 14, and 21. Their colonic contents were collected for microbiome analyses and their colonic epithelia underwent transcriptome analyses. Pseudo-germ-free mice were gavaged with fecal bacteria from heat-stressed and control pigs on the collection days to determine whether gut microbiomes and immune responses resembling those in the pigs could be induced in the mice. Heat-stressed pigs presented with fever and diarrhea from day 7 and their colonic villus length, crypt depth/width, and goblet cell number were significantly lower than those of the controls. Their TLR4, TRAF6, and nuclear p65 were upregulated at the RNA and protein levels. Their proinflammatory IL-6, IL-8, and IL-17 were also upregulated. Colonic microflora composition in the heat-stressed pigs markedly differed from that of the controls. By day 14, the former presented with substantial increases in opportunistic pathogens such as Campylobacterales , Veillonellaceae , and Megasphaera . Intestinal lipopolysaccharide concentrations were higher in the heat-stressed than the control pigs. Mice administered fecal transplantation from heat-stressed pigs had a distinctly different colonic microflora composition from those receiving control pig fecal transplantation. Bacteroides were significantly diminished and Akkermansia were significantly augmented in mice administered feces from heat-stressed pigs for 14 d. In the colonic tissues of mice given feces from heat-stressed pigs, the TLR4/NF-κB signaling pathway was activated and there was a mild inflammatory response. Conclusion Heat stress promotes changes in gut microflora composition which, in turn, activates the TLR4/NF-κB signaling pathway and causes inflammatory bowel disease in pigs.

Background

Inflammatory bowel disease (IBD) affects > 3.1 million people in the United States and 2.5 million in Europe annually. Its incidence is increasing worldwide, especially in East Asia and South Asia [1, 2]. IBD characterized by chronic intestinal inflammation as well as extraintestinal symptoms triggered by genetic predisposition and environmental factors [3]. Various stressors alter the so-called ‘brain-gut axis’ and contribute to a broad array of gastrointestinal disorders including IBD. Hypo- and hyperthermia may aggravate IBD by an unknown mechanism. Furthermore, climate change is increasing the incidence and duration of summertime heat waves in many countries [4]. Mean temperature and relative humidity have risen by ≤ 10.1% and ≤ 1.8%, respectively. Studies have shown that heat stress (HS) induces intestinal mucosal inflammation and damage in pigs [5], chickens[6] , and rats [7].

Cell membranes constitute part of the innate mammalian immune system. They function as gatekeepers and express Toll-like receptors (TLR) in response to the presence of microbial pathogens including

bacteria, viruses, and parasites. TLR4 recognizes lipopolysaccharides (LPS) which abound in the cell walls of Gram-negative bacteria, then a conformationally change and intracellular Toll-interleukin receptor domains containing adaptor molecules are recruited. These adaptors associate with the TLR4 cluster via homophilic interactions between receptor domains. Consequently, activated the n*uclear factor* kappa-light-chain-enhancer of activated B cells (NF-κB) protein complex and mitogen-activated protein kinase (MAPK), resulted various inflammatory cytokine produce [8-12].

TLR4 occurs in the peripheral lymphatic endothelial cells of the small intestine and can be found on the surfaces of the intestinal epithelial cells in IBD patients [13]. An earlier study showed that the number of TLR4 Asp299Gly polymorphism alleles was significantly higher in IBD patients than healthy controls [14]. After the TLR4/NF-κB signaling pathway was inhibited in mice with LPS-induced colitis, colonic IL-6 and TNF-α were significantly downregulated and the mucosa gradually self-repaired [15]. Therefore, TLRs mediate NF-κB activation, participate in the inflammatory response, and cause changes in the IL-6 and IL-8 levels[16-18]. TLR4/MyD88/p65 is upregulated and the number of inflammatory cells is relatively high in the intestinal mucosae of patients with ulcerative colitis. Our previous studies showed that the expression levels of TLR4 and its alternative splicing variants were increased in pigs exposed to HS [19, 20]. However, the role of TLR4 signaling pathway activation in heat stress-induced IBD remains unknown.

The mammalian gastrointestinal tract hosts ~10^{14} microorganisms comprising 500–1,000 unique species and forming synergistic mutualisms with the host [21-24]. Co-evolution of gut microorganisms with their hosts has resulted in specialization of the roles of different microbes in digestion, nutrient utilization, toxin removal, pathogen protection, and regulation of the endocrine and immune systems [25-27]. A healthy intestinal microbe community is diverse, stable, resistant to minor changes, and resilient [28]. Human and mouse studies have shown that gut dysbiosis or disequilibrium of the microbial community is associated with various acute and chronic inflammatory conditions, bowel diseases, metabolic syndromes, and diabetes [29]. Gut dysbiosis and reduced gut microbial ecosystem complexity are common symptoms in patients with Crohn's disease or ulcerative colitis. Nevertheless, it is unknown whether these alterations are causes or consequences of these diseases [30]. It has been reported that fecal microbial transplantation (FMT) successfully treats relapsed Clostridium difficile infections that are ineffective with antibiotics; FMT seems to be beneficial for some patients for other gastrointestinal diseases such as IBD, IBS, etc. , and its effects may through specific microorganisms or its active products to adjust the intestinal flora to treat diseases, but its mechanism of action needs to be explored [31].

Pigs and humans have anatomical, physiological, and immunological similarities. Thus, studies of the immunological mechanisms in pigs could be reproducible in humans. Moreover, pigs have similar susceptibilities and clinical manifestations in response to pathogens causing certain human intestinal disorders [32, 33]. Xiao et al. reported that the homology between human and pig microbiomes is low at the gene level but significantly higher at the level of Kyoto Encyclopedia of Genes and Genomes (KEGG) orthology functions, and greater similarity between human and pig microbiomes than that between

human and mouse microbiomes. Furthermore, ~96% of the functional pathways described in the human gut microbiome resemble those of the pig [34]. The aim of this study was to elucidate the roles of intestinal microbial composition and the TLR4/NF-κB signaling pathway in IBD development in heat-stressed pigs. To this end, we conducted FMT from pigs to mice and examined the inter-species effects.

Results

Clinical signs in pigs

The average forehead temperature of the HS group sharply increased on day 3 and reached 37.77 °C which was 1.03 °C higher than that for the control group. The average rectal temperature on day 3 was 40.46 °C which was 2.84 °C higher than that for the control group. By day 21, the average forehead temperature of the HS group had gradually declined but was still significantly higher than that for the control group. In the latter, the average rectal temperature was 0.88 °C higher than average forehead temperature. For the HS group, however, the average temperature difference was 2.69 °C (Fig. 1a-b). The weight gains in the HS group were 6.41%, 61.30% ($P < 0.01$), and 88.71% ($P < 0.01$) lower than those for the control group at days 7, 14, and 21, respectively (Fig. 1c). The Diarrhea Index for the control group was < 3 and the pigs showed no symptoms of diarrhea. In the HS group, though, diarrhea was observed on day 7 and gradually increased thereafter. The Diarrhea Index from days 8 to 19 was > 3. Diarrhea was most severe on days 11 and 15 and the Diarrhea Index scores were 5.5 and 5.6, respectively (Fig. 1d).

Histopathology of colonic mucosa in pigs

Morphological observation of the colon revealed that the mucosal layer of the control group was intact and no epithelial cells were shed. In contrast, sustained HS caused epithelial cell sloughing, vasodilation, and mucosal hyperemia in the colonic intestinal epithelium from day 7 onwards (Fig. 2a). The crypt depth for the HS pigs became shallower and by day 14 it was significantly different ($P < 0.05$) from the controls (Fig. 2b). In the HS pigs, the number of goblet cells per unit area was markedly lower than that for the control pigs. The difference between groups was significant by day 7 ($P < 0.05$) (Fig. 2c). The number of immune cells between the epithelial cells was also greater in the HS than the control pigs.

Transcriptome of pig colonic tissue

A total of 727,469,990 raw reads were obtained from sample sequencing and 675,459,262 clean reads (Table 1) were generated by double-ended read splicing and filtration (Fig. 3). Superposition of gene coverage reflects whether the sequences are evenly distributed. The plot in Fig. 3a shows that the sequencing results for each sample were not biased. A principal components analysis (PCA) showed strong similarity between samples and the differences between groups were small (Fig. 3b). A heatmap showed that the gene expression levels and their correlation coefficients between samples were high for

the HS test (Fig. 3c). A differential expression volcanic plot (Fig. 3d) revealed that the expression levels of 14,968 genes in the HS samples on day 7 were significantly different from those for the controls. There were 7,163 upregulated and 7,705 downregulated genes in the HS pigs. On day 14, there were 15,036 differentially expressed genes (DEGs) of which 7,114 were upregulated and 7,922 were downregulated (Fig. 3e). KEGG enrichment analysis disclosed that the top 20 signaling pathways of differential gene enrichment included IBD, IL-17, TLR, and cytokine-cytokine receptor interaction (Fig. 3f). A transcriptomic analysis showed that HS induces the TLR4/NF-κB signaling pathway and significantly upregulates TLR4, MyD88, NF-κB, IL-17α, and IL-8 (Fig. 3g-i).

TLR4/NF-κB signaling pathway in pig colon

In the HS pig colons, TLR4 was significantly upregulated on day 1 and peaked by day 7 ($P \leq 0.05$) at which time its expression level was 21.43% higher than it was at day 1 (Fig. 4a, b). There was no significant difference in MyD88 expression (Fig. 4a, c). For the HS group, TRAF6 was significantly upregulated on day 1 and peaked by day 7 ($P \leq 0.05$) at which time its expression level was 12% higher than it was at day 1 (Fig. 4a, d). There were no changes in the expression levels of p65 in the nucleus or extranuclear cells of the control group. Nevertheless, in the HS pigs, nuclear p65 expression was markedly increased relative to the control group. The p65 expression was highest on day 1 and gradually decreased thereafter (Fig. 4a, e-f). For the control group, colonic mucosal cells whose nuclei were expressing p65 were mainly distributed near the side of the intestinal epithelial cells and the expression levels did not significantly (P>0.05) differ across time points. For the HS pigs, p65 expression in the nuclei of the anal and cecal mucosal cells near the intestinal lumen increased in the early stages and decreased thereafter (Fig. 4g).

In the HS pigs, the relative expression of IL-6 mRNA was significantly elevated ($P < 0.01$) by day 7 but significantly declined ($P < 0.05$) thereafter (Fig. 4h). The relative expression of IL-8 mRNA was significantly lower in the HS group than the control group on days 1 ($P < 0.001$), 7 ($P < 0.001$), 14 ($P < 0.05$), and 21 ($P < 0.001$) (Fig. 4i). For the HS pigs, IL-17 mRNA was significantly upregulated on days 7 ($P < 0.001$) and 14 ($P < 0.001$) (Fig. 4j).

The fecal LPS concentrations in the HS pigs were significantly higher on days 1, 7, and 14 than they were for the controls (Fig. 4k). Western blot revealed that for the HS pigs, TLR4 expression was markedly elevated after treating IPEC-J2 cells with 10 μg mL^{-1} LPS for 3 h (Fig. 4k). The nuclear p65 markers were also significantly upregulated ($P < 0.001$) (Fig. 4m).

Pig colonic microbiome

The Illumina HiSeq and paired-end methods used to sequence the 16S and 18SrRNA constructs generated 7,249,898 read pairs. After double-ended read splicing and filtering, 5,362,329 clean tags were generated. The average number of clean tags per sample was 335,146 (Table 2). The Shannon index plot disclosed that each sample curve was flat. Thus, there was sufficient sequencing data and the number of OTU species would not increase with sequencing quantity (Fig. 5). Each sample had numerous OTU and was rich in species. Most species were detected in the samples (Fig. 5a). The rank abundance curves showed that the microbial species richness and the uniformity of species composition for the HS group on days 7, 14, and 21 were lower than those for the control group (Fig. 5b). The PCA indicated that the samples in the control group were highly similar and equidistant whereas those of the HS group had relatively greater similarity (Fig. 5c-d). Compared with the control group, by day 7 in the HS group, the numbers of *Bacteroidetes*, *Firmicutes*, *Spirochaetae,* and *Proteobacteria* had increased. By day 14, the numbers of *Firmicutes* and *Bacteroidetes* had decreased in the HS group while the numbers of *Spirochaetae, Proteobacteria,* and *Tenericutes* had increased (Fig. 5e). Within the *Firmicutes,* it was mainly the numbers of *Lactobacilli* and *Ruminococcaceae* that had changed. Significant changes in the numbers of *Spirochaetae* were reflected in *Treponema 2.* Among the *Bacteroidetes*, the numbers of *Alloprevotella*, *Rikenellaceae,* RC9 gut group*,* and *Prevotellaceae* had changed. By day 14, the *Firmicutes* bacteria comprised mostly *Lactobacillus,* the numbers of *Ruminococcaceae* had slightly declined, and among the *Spirochaetes,* the numbers of Gram-negative *Treponema* had significantly increased. The numbers in the genus *Bacteroides* had diminished because of a decline in the numbers of *Prevotellaceae* (Fig. 5f). A QIIME analysis of four phylogenetic trees demonstrated that the genus *Proteobacteria* in the HS pigs consisted mainly of *Campylobacter* by day 14. This microbe may have been responsible for the diarrhea in HS pigs (Fig. 5g). The LEfSe analysis showed that the relative differences in microflora between the HS and control pigs on day 14 reflected increases in the numbers of opportunistic pathogens such as *Campylobacterales*, *Veillonellaceae*, and *Megasphaera* (Fig. 5h). The KEGG plot revealed that on day 7, the HS pigs presented with relative changes in cell function and metabolism and by day 14, the comparative differences in signaling and environmental adaptation had also increased (Fig. 5i-j).

FMT on mouse colonic microbiome

Following FMT, the paired-end method was used to sequence the 16S and 18S rRNA constructs. Sample sequencing generated 2,866,688 read pairs. After double-ended read splicing and filtering, 2,430,548 clean tags were generated and the average number of clean tags per sample was 62,322 (Table 3). The Shannon index plot disclosed that each sample curve was flat, there was adequate sequencing data, and the number of OTU species should not increase with sequencing quantity. Each sample presented with numerous OTU and abundant species. Most species were detected in the samples (Fig. 6a). The rank abundance curve showed that the species richness and uniformity of species composition were lower in the experimental group than the control group (Fig. 6b). The PCA indicated that the samples in the control group (PBS infusion) had high similarity and were equidistant whereas the samples in the HS group (HF7, HF14; HS pig feces infusion) had even higher similarity (Fig. 6c, d). Seven days after FMT, the numbers of

Bacteroidetes and *Firmicutes* in the HF7 and HF14 groups had increased relative to the CF group infused with feces from control pigs. The numbers of *Bacteroidetes* had changed significantly ($P < 0.05$) and the numbers of bacteria such as *Verrucomicrobia* and *Proteobacteria* had increased (Fig. 6e). The changes in the numbers of *Firmicutes* were explained mainly by *Lactobacillus* and *Turicibacter* while the increase in the numbers of *Bacteroidetes* was primarily the result of changes in the numbers of *Rikenellaceae* and *Prevotellaceae*. *Verrucomicrobia* and *Akkermansia* were increased in the HF7 and HF14 mice (Fig. 6f). Therefore, the composition of the intestinal microbiota in the HF mice had changed following FMT (Fig. 6g, h). ANOVA showed that the intergroup differences in the numbers of *Akkermansia, Bacteroides, Faecalibaculum, Parasutterella,* and uncultured_bacterium_f_*Bacteroidales*_S24-7_group were highly significant ($P < 0.001$) (Fig. 6i). The KEGG plot revealed relative differences in lipid metabolism and xenobiotic biodegradation and increases in signal transduction for HF7 and HF14 (Fig. 6j).

Histopathology of mouse colonic mucosa following FMT

After FMT, lymphocyte infiltration and tissue gaps were observed in the colonic mucosae of the HF1, HF7, and HF21 mice compared with the CF group (Fig. 7a). Goblet cell and mucosal epithelial shedding had comparatively decreased in the HF14 group (Fig. 7a, d). Compared with the control, the colonic villi were significantly shorter in the H14 mice ($P < 0.05$) (Fig. 7b) and the intestinal muscle layer was significantly thinner ($P < 0.05$) (Fig. 7c).

Colon transcriptomes of mice administered FMT

We obtained a total of 944,841,602 raw reads from the sample sequencing and 932,528,258 clean reads from double-ended read splicing and filtration (Table 4). Superposition of gene coverage indicates whether the sequences obtained are evenly distributed within the gene. The plot presented no obvious biasing front. Thus, the sequencing results for each sample were not biased (Fig. 8a). The expression levels of 19,017 genes in the CF7 and HF7 mice were significantly ($P < 0.001$) different. There were 9,494 upregulated, 9,523 downregulated genes, and 36 significant ($P < 0.001$) differentially expressed genes (DEGs) between the HF7 and CF7 mice (Fig. 8b). There were 19,019 DEGs of which 9,275 were upregulated, 9,744 were downregulated and 61 were significantly ($P < 0.05$) differentially expressed in HF14 compared to CF14 (Fig. 8c). Transcriptomics showed that FMT induced TLR4, MyD88, and NF-κB in the TLR4/NF-κB signaling pathway and they were significantly ($P < 0.001$) upregulated compared with the PBS group. However, there were no significant changes in the relative expression levels of the proinflammatory factors (Fig. 8d-f). The TLR4/NF-κB signaling pathway in the HF14 mice was partially activated compared to that of the CF14 group (Fig. 8g). The KEGG enrichment analysis disclosed that the B-cell receptor signaling pathway, intestinal immune network for IgA production, NF-κB, and cytokine-cytokine receptor interactions were significantly ($P < 0.05$) upregulated in the HF mice (Fig. 8h-i).

TLR4/NF-κB signaling pathway in FMT mouse colon

TLR4 was significantly ($P < 0.001$) upregulated in the HF1 mice and its expression level was highest for the HF7 mice (Fig. 9a, b). There were no significantly ($P > 0.05$) changes in nuclear p65 expression in the CF groups. In contrast, nuclear p65 expression in the HF groups was significantly ($P < 0.001$) upregulated compared with the CF groups. The highest nuclear p65 expression levels were determined for the HF7, HF14, and HF21 mice (Fig. 9a, c-d).

Discussion

Interactions between genetically predisposition and environmental factors in inappropriate host immune responses to intestinal microflora are important factors in inflammatory bowel disease (IBD) pathogenesis including Crohn's disease and ulcerative colitis. The roles of stress-induced gut mucosal pathophysiology have not been fully elucidated. However, recent evidence has indicated that chronic stress may be implicated in disease development [35]. Here, we established a chronic HS-induced IBD model and found that Gram-negative intestinal bacteria play essential roles in the intestinal inflammatory response mediated by the TLR4/NF-κB signaling pathway.

In pigs, heat stress diverts blood to the periphery and maximizes radiant heat dissipation. Nevertheless, this response causes vasoconstriction in the gastrointestinal tract [36], hypoxia in the intestinal epithelium because of the reduced blood supply, reductions in nutrient flow, and compromised intestinal integrity and function[37]. Pearea et al. [38] found that exposure to 37 °C for 4 h can damage the intestinal mucosa of growing pigs. After 6 h at 37 °C, large numbers of intestinal epithelial cells were sloughed and there was severe submucosal congestion and edema. The HS pigs in the present study showed thinner intestinal walls, shorter intestinal villi, and shallower crypts than the controls. Other stressors such as psychosocial events in humans [35], cold stress [39], and restraint stress in mice [40] strongly induced inflammatory responses in the gut. Therefore, HS-induced vasoconstriction and hypoxia in the gastrointestinal tract do not fully explain IBD in pigs and another mechanism may be involved in this pathogenesis.

The gastrointestinal tract is tightly controlled by the immune and neuroendocrine systems. Stress mitigation significantly improved gut homeostasis in pigs [41, 42]. Destruction of the epithelial layer and thinning of the protective mucus layer may create conditions conducive to bacterial invasion of the mucosae and the blood vessels [43-46]. Bacterial products such as LPS are recognized by intestinal epithelial cells (IEC) via TLR4. TLR4 upregulation in the gut enhances the ability of the body to recognize antigens. Nevertheless, sustained stress may trigger an inflammatory response [47]. Pearce et al. [48] showed that HS and reduced feed intake compromised intestinal lining integrity and increased endotoxin permeability in pigs. Here, TLR4 expression was upregulated in heat stressed pigs not only in protein level, but in transcript level, suggested that TLRs signal pathway may play an important role in intestinal inflammation induced by heat stress.

The nuclear transcription factor p65 induces inflammatory genes after it is translocated to the nucleolus. When rats were maintained at 42 °C, their p65 activity was significantly increased relative to a control group exposed to an ambient temperature of 25 ± 3 °C and their IL-1β was also dramatically upregulated [44]. Two hours of heat stress in pigs can significantly increase blood TNF-α levels and inhibit lysozyme production. Numerous macrophages accumulate at the inflammation site and produce the proinflammatory cytokines IL-6 and IL-8 that mobilize lymphocytes and other immunocytes in the inflammatory process [49, 50]. Upregulation of proinflammatory cytokines triggers an acute phase reaction presenting with fever, anorexia, and hormonal and metabolic changes [51]. Here, we found that IL-17 was also significantly upregulated in the HS pig colon. All of the aforementioned factors contribute to IBD development and progress, suggested that the TLR4/TRAF6/NF-κB signaling pathway plays a vital role in HS-induced IBD pathogenesis.

There are numerous microorganisms in the intestinal tract and the epithelial cells comprise the first-line protective barrier [52, 53]. Here, diarrhea increased in intensity in HS pigs by day 14 when the numbers of opportunistic Gram-negative bacterial pathogens such as *Campylobacterales*, *Veillonellaceae* and *Megasphaera* increased in the intestinal microflora. Oxidative stress is associated with host heat or cold stress [54] and may generate reactive oxygen species (ROS). The bacteria residing on the colonic mucosa have relatively greater oxygen tolerance [55], it might favor the proliferation of aerotolerant phyla in the gut such as *Actinobacteria* and *Proteobacteria*. On the other hand, gut microbiota can directly or indirectly contribute to ROS production via the mucosal cells [56] . *Helicobacter pylori* generates ROS and induces neutrophils to produce them as well [57]. *Helicobacter pylori* also enhances nitric and nitrous oxide production by activating macrophages [58]. As there is an interaction between inflammation and microflora, further studies are required to discern whether the observed intestinal microflora dysbiosis in the HS pigs was triggered by inflammation.

The intestinal microbial composition changed in the HF mice after FMT pig feces administration. Relative to the untreated mice, the HF mice presented with fewer goblet cells, shorter intestinal villi, and thinner muscle layers. Therefore, an inflammatory response had developed in the intestines of the FMT-treated HF mice. Moreover, the TLR4/NF-κB signaling pathway was activated in both the H7 and H14 mice. Breitruck et al. [59] reported that the intestinal mucosal structure is damaged in mice with IBD. This injury is characterized by severe bleeding and IL-6 and IL-10 upregulation. However, in the present study, the proinflammatory factors were not upregulated in mice administered the FMT possibly because of large numbers of *Akkermansia muciniphila* in the mouse intestinal tract. This microbe is a Gram-negative, mucin-degrading bacterium residing in the human and animal gastrointestinal tract. It can induce IL-8 production in the intestinal cells to a level 100-fold higher than that promoted by *Escherichia coli.* Thus, *A. muciniphila* has relatively weak proinflammatory activity in intestinal epithelial cells [60]. Diao et al. reported that gut microbiota affected certain pig traits and transferred their phenotypes to mice receiving pig feces via a different mechanism [61]. The gut microbiota also influenced epithelial cell morphology and renewal rates, intestinal nutrient digestion and absorption, and the gut barrier [5, 61].

In our study, the relationship between changes in pig intestinal microbes and activation of the TLR4/NF-κB pathway under heat stress was explained by FMT. It also shows the use of live microorganisms, such as FMT, has potential therapeutic value for the disease, but the risks involved must also be considered. FMT can restore intestinal flora diversity, treat diarrhea caused by Clostridium difficile, and avoid drug resistance caused by long-term use of antibiotics, but it may also spread or increase susceptibility to intestinal bacteria-related diseases[62]. FMT alters bacteria composition and establishes trans-kingdom equilibrium between gut fungi, viruses and bacteria to promote the recovery of microbial homeostasis. FMT is not a one size fits all and studies are required to identify microbial components that have specific effects in patients with different diseases[63].

Conclusions

The present study showed that HS-induced intestinal dysbiosis disrupted gut microflora composition, increased the numbers of opportunistic, pathogenic Gram-negative bacteria, activated the TLR4/NF-κB signaling pathway, and promoted proinflammatory cytokine production. This process triggered an inflammatory response and compromised the intestinal barrier. This study enhanced our understanding of stress-induced IBD and the increase in diarrhea in mammals subjected to prolonged humid heat in the summertime.

Methods

Animals and management

The experimental protocols involving the management and care of pigs and mice were approved by the Animal Care and Use Committee of Guangdong Ocean University, Zhanjiang, China (Permit No. 206-1108).

Pig study

Twenty-four pigs (Luchuan sows × Duroc boars; 12 males and 12 females) each weighing 15 ± 2 kg were housed in two animal rooms at the Animal Hospital of Guangdong Ocean University, Zhanjiang, China. The pigs were randomly divided into two animal room groups. Each group had six males and six females of similar body weight. There were four replicates (collection dates) of three per group. The animals were maintained for 2 wks at 20 ± 2 °C and RH = 75–85% to acclimatize them to the environment. The photoperiod was maintained under 12-h light / 12-h darkness over the adaptation and trial periods. Throughout the study, the pigs were fed a complete formula in the morning, afternoon, and evening with ~6-h intervals between feedings. Drinking water was freely available. To minimize acute heat stress, the animal facility was gradually warmed over a 7-d period. The trial lasted 21 d. The control animals were subjected to 25 ± 3 °C and the HS animals were exposed to 34 ± 1 °C at 75–85% RH.

Mouse study

Pseudo-germ-free animals (SPF grade) were induced by feeding mice (*n* = 130) with a mixture of vancomycin (200 mg kg^{-1}), metronidazole (200 mg kg^{-1}), and neomycin (200 mg kg^{-1}) for 5 d consecutively. Throughout the study period, all mice were maintained under a 12-h light / 12-h dark photoperiod and an air circulation cycle under the Exhaust Ventilated Closed-System Cage Rack. They had *ad libitum* access to autoclave-sterilized chow and water.

Ten mice were controls (BC group) and received only chow and *ad libitum* water. The other mice (*n* = 120) were divided into four groups of 30 each. They were administered FMT after pig feces collection on days 1, 7, 14, and 21, respectively. Each group was further subdivided into three treatment groups of 10 mice each. They were administered intragastric infusions of either phosphate-buffered saline (PBS group), a 0.5-mL mixture of control pig feces homogenized in PBS (CF group), or a 0.5-mL mixture of HS pig feces homogenized in PBS (HF group). All mice were sacrificed by break the neck after ether anesthesia 7 d after the intragastric infusion.

Sample collection

All pigs were observed for diarrhea and weight gain. Fecal shape and color were recorded daily and scored [66] as indicated in Table 5. The Diarrhea Index was calculated according to the scores for six pigs sacrificed at each sampling time.

$$\text{Diarrhea Index} = \text{sum of scores} / 6 \quad (1)$$

Forehead and rectal temperatures were measured daily with a far-infrared thermometer. At each sampling time (days 1, 7, 14, and 21), pigs from the control (*n* = 3) and treatment groups (*n* = 3) were electric shock to sacrificed. Colonic feces and colon tissue samples were collected and immediately stored at -80 °C until the subsequent cell culture studies, microbiome and transcriptomic analyses, and mouse FMT studies. After FMT administration, mice (*n* = 30 per collection day) were sacrificed on day 7. Blood, colonic feces, and colon tissue samples were collected and immediately stored at -80 °C until the subsequent analyses.

Statistics

The data were subjected to *t*-tests using SPSS v. 21.0 (IBM Corp., Armonk, NY, USA). Data are expressed as means ± standard deviation. $P \leq 0.05$ indicates significant difference. $P \leq 0.01$ indicates highly significant difference.

Analyses

Morphological observations

Colonic tissue was fixed in buffered formalin (10% v/v) and stained with H&E for histopathological examination. Image-Pro Plus v. 6.0 (Media Cybernetics Inc., Silver Spring, USA) was used to measure villus height, crypt depth, and width[64]. Hydrated colonic tissue sections were treated with amylase at 37 °C for 1 h, rinsed under running water for 10 min, and stained with periodic acid solution at room temperature (25 °C) for 7 min according to the instructions for the Glycogen D-PAS Staining Kit (Leagene Biotechnology, Beijing, China). The tissue sections were rinsed with tap water, immersed in Schiff's reagent in the dark for 15 min, and rinsed with tap water for 10 min to remove the stain. The sections were dehydrated with an alcohol concentration gradient (75%, 85%, 95%, and then 100%), cleared of alcohol with xylene, and sealed with neutral gum. Image-Pro Plus v. 6.0 (Media Cybernetics Inc., USA) was used to evaluate the goblet cells per unit area in the colonic mucosa [65].

Western blot analysis

To measure the responses of the critical TLR4/NF-κB signaling pathway proteins in the colonic tissues, total protein was extracted with RIPA (radioimmunoprecipitation assay) lysis buffer (Beyotime, China) and the nuclear and cytoplasmic protein fractions were extracted with NE-PERTM nuclear and cytoplasmic extraction reagents (Thermo Fisher Scientific, USA), respectively. The total protein concentrations were determined using a BCA (bicinchoninic acid) protein assay kit (CWBIO, China). Equal amounts of protein lysate were separated by sodium dodecyl sulfate-polyacrylamide gel electrophoresis and electrotransferred to nitrocellulose membranes (Merck Millipore, Germany). The membranes were blocked for 1 h with 5% skimmed milk powder and incubated with primary antibody of Anti- TLR4, TRAF6, MyD88, p65 (Abcam, USA) and β-actin (Beyotime China overnight at 4 °C. The blots were incubated under the temperature of 4°C for 2h with a corresponding secondary antibody conjugated to horseradish peroxidase (HRP). Positive bands were visualized by enhanced chemiluminescence (ECL; Tanon, China). The band intensities were semi-quantitatively analyzed by densitometry with Gel-Pro Analyzer v. 4.0 (Meyer Instruments, Houston, TX, USA). The relative protein expression levels were normalized to β-actin. Antibodies against TLR4, TRAF6, MyD88, p65, and β-actin were obtained from Abcam (Cambridge, UK).

HRP-conjugated anti-rabbit IgG and anti-mouse IgG were obtained from Cell Signaling Technology (Danvers, USA).

TLR4, MyD88, and TRAF6

Paraffin sections of the intestinal tissues were prepared. TLR4-, MyD88-, and TRAF6-positive cells and p65 (NF-κB) activity were detected by immunohistochemistry (IHC). Data are expressed as means ± standard deviation. One-way ANOVA and Tukey's multiple comparisons test were performed on the data in SPSS v. 21.0 (IBM Corp., Armonk, NY, USA). $P \leq 0.05$ indicates significant difference and $P \leq 0.01$ indicates highly significant difference.

Detection of p65 protein entry into the nucleus

Frozen intestinal tissue sections (8 μm) stored at -80 °C were fixed in 4% (v/v) paraformaldehyde for 10 min, rinsed thrice with PBS for 2 min each time, and blocked with 1% (v/v) bovine serum albumin (BSA) for 1 h. The p65 primary antibody was diluted 1:100 and 100 μL of it was added to each tissue section. These were stored in the dark overnight at 4 °C. The tissue sections were then rinsed thrice with PBS (pH 7.4) for 10 min each time. Alexa Fluor 647-labeled goat anti-rabbit IgG (H+L) (Beyotime China). To measure the responses of the critical TLR4/NF-κB signaling pathway proteins in the colonic tissues, total protein was extracted with RIPA (radioimmunoprecipitation assay) lysis buffer (Beyotime , China) and the nuclear and cytoplasmic protein fractions were extracted with NE-PERTM nuclear and cytoplasmic extraction reagents (Thermo Fisher Scientific, Waltham, USA), respectively. The total protein concentrations were determined using a BCA (bicinchoninic acid) protein assay kit (CWBIO, China). Equal amounts of protein lysate were separated by sodium dodecyl sulfate-polyacrylamide gel electrophoresis and electrotransferred to nitrocellulose membranes (Merck Millipore, Germany). The membranes were blocked for 1 h with 5% skimmed milk powder and incubated with primary antibody of Anti- TLR4, TRAF6, MyD88, p65 obtained from Abcam (Cambridge, UK) and β-actin (Beyotime, China) for 12 h at 4 °C. The blots were incubated under the temperature of 4°C for 2h with a corresponding secondary antibody of HRP-conjugated anti-rabbit IgG and anti-mouse IgG were obtained from Cell Signaling Technology (Danvers, MA, USA) conjugated to horseradish peroxidase (HRP). Positive bands were visualized by enhanced chemiluminescence (ECL; Tanon, China). The band intensities were semi-quantitatively analyzed by densitometry with Gel-Pro Analyzer v. 4.0 (Meyer Instruments, Houston, TX, USA). Alexa Fluor 647-labeled goat anti-rabbit IgG (H+L) (Beyotime, China) was diluted 1:1,000 and added dropwise to the tissue sections which were then incubated in an opaque wet box for 1.5 h. The tissue section slides were then rinsed thrice with PBS (pH 7.4) for 10 min each time, immersed in 4’,6-diamidino-2-phenylindole (DAPI) fluorescent stain for 10 min, and rinsed thrice in PBS for 10 min each time. The slides were then mounted with anti-quenching sealer and photographed under a fluorescence microscope (Olympus BX51, Japan).

Microbial genomic sequencing and analysis

Total genomic DNA was extracted from the samples with a QIAamp DNA Stool Mini Kit (Qiagen, Germany) according to the manufacturer's instructions. DNA concentration and purity were evaluated on 1% agarose gels. The quantity of DNA was determined with a NanoDrop 1000 spectrophotometer (Thermo Fisher Scientific, USA) after zeroed with sample solvents and the DNA was diluted to 1 ng μL^{-1} with sterile water. The V3-V4 distinct regions of the 16S rRNA genes were amplified with specific barcoded primers[66, 67]. The PCR reactions were performed in triplicate in a total volume of 25 μL consisting of 1μL of each the primers (5 μM), 10 μL of 10 ng DNA template, 4 μL of 1×FastPfu buffer, 1μL of 2.5 mM dNTPs, 0.4 μL FastPfu polymerase, and 7.6 μL nuclease-free water.

The PCR program was as follows: initial denaturation at 94 °C for 5 min, 30 cycles at 94 °C for 50 s, 55 °C for 30 s, 72 °C for 50 s, and a final extension at 72 °C for 6 min. The PCR products were purified with an AxyPrep DNA Gel Extraction Kit (Axygen Scientific, USA). Amplicons from all samples were sent to a commercial company (Biomarker, China) for sequencing on an Illumina HiSeq 2500 platform (Illumina, USA). Species classification information corresponding to each OTU was obtained by comparing the representative OTU sequence with the microbial reference database. Sample community compositions were calculated at the phylum, class, order, family, genus, and species levels and generated in QIIME (Version 1.8.0). GraphPad Prism v. 6.0c (GraphPad Software, USA), R v. 3.0.3, Metastats, and STAMP (Statistical Analysis of Metagenomic Profiles) were used for the statistical analyses. The weighted UniFrac distances among the groups were statistically compared by analysis of similarities in the 'vegan' package of R v. 3.0.3. In the univariate analysis of gut microbiota and predicted KEGG biochemical pathways for each group, one-way ANOVA with Bonferroni's multiple comparison test was performed to compare the alpha diversities among the groups. Metastats identified differentially abundant phyla, genera, and species in the groups. Significant differences between groups were identified by the LEfSe (line discriminant analysis effect size) method.

Transcriptome sequencing and analysis

An enzyme-free cryopreservation tube was pre-cooled in liquid nitrogen and colonic epithelium was quickly excised and cut into pieces similar in size to soybean granules. RNase-free water was used to prepare 1 × PBS or saline, the tissue surface stains were quickly removed, and the surface liquid was absorbed and collected in the cryopreservation tube which was rapidly transferred to liquid nitrogen and sent to Majorbio Bio-farm Technology Co. (Shanghai, China) for sequencing. The eukaryotic mRNA sequencing was based on the HiSeq platform used to sequence all mRNAs transcribed at specific times from specific eukaryote tissues. Total RNA was extracted from the tissue samples and its concentration and purity were detected with a Nanodrop 2000 spectrophotometer (Thermo Fisher Scientific, Waltham, MA, USA) after zeroed with sample solvents. RNA integrity was assessed by sodium dodecyl sulfate

polyacrylamide agarose gel electrophoresis (SDS-PAGE) and the RNA integrity number was determined with an Agilent 2100 Bioanalyzer (Agilent Technologies, Santa Clara, CA, USA). The eukaryotic mRNA 3'-end had a polyA tail structure. Magnetic beads treated with Oligo (dT) were used for A-T base pairing with flo A and mRNA isolated from the total RNA for transcriptome analysis. Fragmentation buffer was added to break the mRNA into small ~300-bp fragments. Six-base random hexamers were added by reverse transcription and mRNA was used as a template to reverse the synthesis of one-strand cDNA and for two-strand synthesis to form a stable double-stranded structure. The short fragments were connected to the adaptor sequence and then sequenced on the Illumina HiSeq platform (Illumina, USA). A single Illumina sequencing run generated billions of reads. Statistical methods were used to measure the sequences visually reflecting library construction and sample sequencing quality. Quality of the data after the quality control (reads) was compared against the reference genome to obtain mapped data (reads) for the subsequent analysis. Quality of the sequencing comparison was also evaluated. Based on existing reference genomes, the mapped reads were assembled, spliced with Cufflinks, and compared against known transcripts, transcripts without annotation information, and functional annotations of potential new transcripts. Read counts for each sample gene/transcript were obtained using featureCounts alignment to genome data and annotation files. Fragments per kilobases per million reads (FPKM; number of reads on one million bases per gene alignment) were calculated. The FPKM method eliminates the effects of differences in gene length and sequencing quantity on gene expression calculation. The calculated gene expression may then be used to compare gene expression differences among samples. After securing the number of read counts for the gene/transcript, analysis of differential gene/transcript expression between samples was performed in the multi-sample (≥ 2) project and the differentially expressed genes/transcripts were identified.

RNA extraction and cDNA synthesis

The synthetic primer sequences (BBI Life Sciences, Shanghai, China) are listed in Table 6. A ~0.5 g tissue block was pulverized in liquid nitrogen and transferred to a 1.5-mL centrifuge tube. Then 1 mL TRIzol reagent (Thermo Fisher Scientific, Waltham, MA, USA) was added and the tube was placed on ice for 20 min. The tube was inverted to ensure complete lysis and prevent sedimentation. Then 200 μL NH_4Cl was added and the tube was vigorously shaken to emulsify the contents. The tube was then left to stand at 25 °C for 5 min and centrifuged with speed in 12000 rpm at 4 °C for 10 mins. The supernatant (200 μL) was transferred to a new centrifuge tube and an equal volume of isopropanol was added. The contents were mixed by inversion, left to stand at 25 °C for 10 min, and centrifuged with speed in 12000 rpm at 4 °C for 10 min. The supernatant was discarded and 1 mL pre-cooled 75% (v/v) ethanol (4 °C) was added. The tube was gently inverted, left to stand for 2 min, and centrifuged at 12,000 × *g* and 4 °C for 5 min. The supernatant was removed and dried at 25 °C for 5 min. Twenty microliters RNase-free water was added to dissolve the RNA and the solution was stored at -80 °C. Then 2 μL RNA mixture was extracted and 1% agarose gel electrophoresis was performed to check its integrity. The rest of the mixture was diluted

100×. Diethyl pyrocarbonate water was used as a blank control and OD_{260}/OD_{280} were measured by OD-1000+ Spectrophotometer (ONE Drop, USA) after zeroed with sample solvents.

After removing genomic DNA, a reverse transcription reaction system was prepared on ice according to the instructions for the HiScript® Q Select RT SuperMix for qPCR (+gDNA wiper) (Vazyme Biotech, Nanjing, China), The PCR program was 25 °C for 10 min, 50 °C for 30 min, and 85 °C for 5 min. After the reaction was completed, the cDNA fractionation apparatus was stored at -80 °C until later use.

Relative quantitative real-time RT-PCR

The RT-qPCR system was configured according to the instructions for the ChamQTM SYBR® qPCR Master Mix Kit (Vazyme Biotech, Nanjing, China) for fluorescence quantitative PCR. The relative expression level was calculated by the $2^{-\Delta\Delta Ct}$ method[68].

Cell culture

The intestinal porcine epithelial cell (IPEC-J2) model was a gift from Dr. Bruce Schultz of Kansas State University. The cells were cultured in Dulbecco's modified Eagle's medium: nutrient mixture F-12 (DMEM/F12; Sigma Aldrich Corp., St. Louis, MO, USA) containing 10% (v/v) fetal bovine serum (FBS), penicillin (100 U mL^{-1}), and streptomycin (100 U mL^{-1}) in a 25-cm, two-cell culture flask (Corning Inc., USA) stored in a humidified incubator at 37 °C and 5% CO_2. When the cells grow to 80% confluence, discard the medium, wash with PBS 2-3 times, add 1ml Trypsin-EDTA (0.25%, Thermo Fisher, USA) for 3 minutes, and then add medium to terminate the treatment. After centrifugation at 1000 rpm for 5 min at room temperature, the supernatant was discarded, diluted with the medium in proportion, and transferred to a 24-well plate. After the cells grew to sub-confluence in 24-well plates, the culture medium was removed and the cells were washed twice with PBS.

In vitro LPS validation experiment

The IPEC-J2 cells were subjected to 10 μg mL^{-1} LPS for 3 h. Western blot was run to detect TLR4 expression and p65 entry in the nucleus. One gram of each fecal sample was weighed out and washed thrice with PBS. The final fecal mass: PBS volume was 1:9. The fecal suspensions were atomized for 15 min with an ultrasonic cell pulverizer (Φ6 horn ultrasonic treatment, 1.5 s; interval, 2 s; power, 25%). After centrifugation at 5,000 × *g* for 10 min under

4 °C, the supernatant was collected for enzyme-linked immunosorbent assay (ELISA).

Abbreviations

ANOVA, analysis of variance; BCA, bicinchoninic acid; BSA, bovine serum albumin; DAPI, 4’,6-diamidino-2-phenylindole; DMEM, Dulbecco’s modified Eagle’s medium; ECL, enhanced chemiluminescence; ELISA, enzyme-linked immunosorbent assay; FBS, fetal bovine serum; FMT, fecal microbiota transplantation; FPKM, fragments per kilobases per million reads; GO, gene ontology; H&E, hematoxylin and eosin staining; HRP, horseradish peroxidase; IBD, inflammatory bowel disease; IHC, immunohistochemistry; KEGG, Kyoto Encyclopedia of Genes and Genomes; LEfSe, line discriminant analysis effect size; LPS; line discriminant analysis effect size; MAPK, mitogen-activated protein kinase; NF-kB, n*uclear factor* kappa-light-chain-enhancer of activated B cells; OTU, operational taxonomic unit; PAS, periodic acid-Schiff staining; PBS, phosphate-buffered saline; PCA, principal components analysis; PCR, polymerase chain reaction; RH, relative humidity; RIPA, radioimmunoprecipitation assay; ROS, reactive oxygen species; RT, room temperature; SDS-PAGE, sodium dodecyl sulfate polyacrylamide agarose gel electrophoresis; TLR, Toll-like receptor

Declarations

Ethics approval and consent to participate

The experimental protocols describing the management and care of animals were reviewed and approved in advance by the Animal Care and Use Committee of Guangdong Ocean University, Zhanjiang, China. All the animals were approved and regulated to house at Guangdong Ocean University Animal Hospital, Zhanjiang, China.

Consent for publication

Written informed consent for publication was obtained from all participants.

Availability of data and material

The datasets used and/or analysed during the current study are available from the corresponding author upon reasonable request.

Competing interests

The authors have no competing or conflicting interests to declare.

Funding

This work was supported by the National Natural Science Foundation of China [grant nos. 31101862, 31472243] and Shenzhen Projects for Basic Research [JCYJ20170306162414058]. The funding bodies had no role in the design of the research, the collection, analysis, and interpretation of data, and the writing of the manuscript.

Authors' contributions

XJ conceived the project and designed the experiments. CH, HY, DG, TY, JL, and LW conducted the experimental work and analyzed the data. XJ and RG interpreted the results. CH and YP prepared the figures and wrote the manuscript. HY and JC edited the manuscript. XL and ZN participated in the enrichment analysis and manuscript writing and revision. All authors read and approved the manuscript content.

Acknowledgements

This work was supported by the National Natural Science Foundation (NSFC) of China [Nos. 31902314 and 31472243], and the Shenzhen Projects for Basic Research [No. JCYJ20170306162414058]. The funding bodies had no role in the design of the research, the collection, analysis, and interpretation of data, or the writing of the manuscript.

Authors' information (optional)

Not applicable

References

1. Dahlhamer JM. Prevalence of Inflammatory Bowel Disease Among Adults Aged ≥18 Years — United States, 2015. Morbidity and mortality weekly report. 2016;65(42):1166.
2. Kaplan, G. G. The global burden of IBD: from 2015 to 2025. Nature Reviews Gastroenterology & Hepatology. 2015.
3. Ananthakrishnan AN, Bernstein CN, Iliopoulos D, Macpherson A, Neurath MF, Ali RA, et al. Environmental triggers in IBD: a review of progress and evidence. Nat Rev Gastroenterol Hepatol. 2018;15(1).
4. Amengual A, Homar V, Romero R, Brooks HE, Ramis C, Gordaliza M, et al. Projections of heat waves with high impact on human health in Europe. Global & Planetary Change. 2014;119:71-84.
5. Pearce SC, Mani V, Boddicker RL, Johnson JS, Weber TE, Ross JW, et al. Heat stress reduces barrier function and alters intestinal metabolism in growing pigs. Journal of Animal Science. 2012;90 Suppl 4(Supplement 4):257-9.
6. Quinteiro-Filho WM, Ribeiro A, Ferraz-de-Paula V, Pinheiro ML, Sakai M, Sa LRM, et al. Heat stress impairs performance parameters, induces intestinal injury, and decreases macrophage activity in broiler chickens. Poultry Science. 2010;89(9):1905-14.
7. Hall DM, Buettner GR, Oberley LW, Xu LJ, Gisolfi CV. Mechanisms of circulatory and intestinal barrier dysfunction during whole body hyperthermia. American Journal of Physiology Heart & Circulatory Physiology. 2001;280(2):H509-21.
8. Brubaker SW, Bonham KS, Zanoni I, Kagan JC. Innate Immune Pattern Recognition: A Cell Biological Perspective. Annual Review of Immunology. 2015;33(1):257-90.

9. Doyle SL, O'Neill LAJ. Toll-like receptors: From the discovery of NFκB to new insights into transcriptional regulations in innate immunity. Biochemical Pharmacology. 2006;72(9):1102-13.
10. Gilmore TD. Introduction to NF-kappaB: Players, pathways, perspectives. Oncogene. 2006;25(51):6680-4.
11. Hayden MS, West AP, Ghosh S. NF-ι[kappa]ιB and the immune response. Oncogene. 2006;25(51):6758-80.
12. Neill LAJB, Andrew G. The family of five: TIR-domain-containing adaptors in Toll-like receptor signalling. Nature Reviews Immunology. 2006;7(5):353-64.
13. Toiyama Y, Araki T, Yoshiyama S, Hiro J-i, Miki C, Kusunoki M. The Expression Patterns of Toll-Like Receptors in the Ileal Pouch Mucosa of Postoperative Ulcerative Colitis Patients. Surgery Today. 2006;36(3):287-90.
14. Perez-Pardo P, Dodiya HB, Engen PA, Forsyth CB, Huschens AM, Shaikh M, et al. Role of TLR4 in the gut-brain axis in Parkinson's disease: a translational study from men to mice. Gut. 2019;68(5):829-43.
15. Li R, Chen Y, Shi M, Xu X, Zhao Y, Wu X, et al. Gegen Qinlian decoction alleviates experimental colitis via suppressing TLR4/NF-κB signaling and enhancing antioxidant effect. Phytomedicine International Journal of Phytotherapy & Phytopharmacology. 2016;23(10):1012-20.
16. Jian C-X, Li M-Z, Zheng W-Y, He Y, Ren Y, Wu Z-M, et al. Tormentic acid inhibits LPS-induced inflammatory response in human gingival fibroblasts via inhibition of TLR4-mediated NF-κB and MAPK signalling pathway. Archives of oral biology. 2015;60(9):1327-32.
17. Fu H, Hu Z, Di X, Zhang Q, Zhou R, Du H. Tenuigenin exhibits protective effects against LPS-induced acute kidney injury via inhibiting TLR4/NF-κB signaling pathway. European journal of pharmacology. 2016;791:229-34.
18. Gao W, Zhao Z, Yu G, Zhou Z, Zhou Y, Hu T, et al. VEGI attenuates the inflammatory injury and disruption of blood–brain barrier partly by suppressing the TLR4/NF-κB signaling pathway in experimental traumatic brain injury. Brain research. 2015;1622:230-9.
19. Ju XH, Xu H-J, Yong Y-H, An L-L, Jiao P-R, Liao M. Heat stress upregulation of Toll-like receptors 2/4 and acute inflammatory cytokines in peripheral blood mononuclear cell (PBMC) of Bama miniature pigs: an in vivo and in vitro study. Animal. 2014;8(09):1462-8.
20. Ju XH, XU H-j, YONG Y-h, AN L-l, XU Y-m, JIAO P-r, et al. Heat Stress Upregulates the Expression of TLR4 and Its Alternative Splicing Variant in Bama Miniature Pigs. Journal of Integrative Agriculture. 2014;13(11):2479-87.
21. Ley, E. R. Obesity alters gut microbial ecology. 2005.
22. Savage DC. Microbial ecology of the gastrointestinal tract. Annual review of microbiology. 1977;31(1):107-33.
23. Xu J, Gordon JI. Honor thy symbionts. Proceedings of the National Academy of Sciences. 2003;100(18):10452-9.

24. Larsson E, Tremaroli V, Lee YS, Koren O, Nookaew I, Fricker A, et al. Analysis of gut microbial regulation of host gene expression along the length of the gut and regulation of gut microbial ecology through MyD88. gut. 2012;61(8):1124-31.
25. Bäckhed F, Ley RE, Sonnenburg JL, Peterson DA, Gordon JI. Host-bacterial mutualism in the human intestine. science. 2005;307(5717):1915-20.
26. Hill DA, Artis D. Intestinal bacteria and the regulation of immune cell homeostasis. Annual review of immunology. 2009;28:623-67.
27. Ley RE, Hamady M, Lozupone C, Turnbaugh PJ, Ramey RR, Bircher JS, et al. Evolution of mammals and their gut microbes. Science. 2008;320(5883):1647-51.
28. Levy M, Blacher E, Elinav E. Microbiome, metabolites and host immunity. Current opinion in microbiology. 2017;35:8-15.
29. Brown K, DeCoffe D, Molcan E, Gibson DL. Diet-induced dysbiosis of the intestinal microbiota and the effects on immunity and disease. Nutrients. 2012;4(8):1095-119.
30. Manichanh C, Borruel N, Casellas F, Guarner F. The gut microbiota in IBD. Nature reviews Gastroenterology & hepatology. 2012;9(10):599.
31. D'Haens GR, Jobin C. Fecal Microbial Transplantation For Diseases Beyond Recurrent Clostridium Difficile Infection. Gastroenterology. 2019.
32. Meurens F, Summerfield A, Nauwynck H, Saif L, Gerdts V. The pig: a model for human infectious diseases. Trends in microbiology. 2012;20(1):50-7.
33. Zhang Q, Widmer G, Tzipori S. A pig model of the human gastrointestinal tract. Gut microbes. 2013;4(3):193-200.
34. Xiao L, Estelle J, Kiilerich P, Ramayo-Caldas Y, Xia Z, Feng Q, et al. A reference gene catalogue of the pig gut microbiome. Nature microbiology. 2016;1(12):16161.
35. Brzozowski B, Mazur-Bialy A, Pajdo R, Kwiecien S, Bilski J, Zwolinska-Wcislo M, et al. Mechanisms by which stress affects the experimental and clinical inflammatory bowel disease (IBD): role of brain-gut axis. Current neuropharmacology. 2016;14(8):892-900.
36. Lambert GP. Stress-induced gastrointestinal barrier dysfunction and its inflammatory effects. Journal of animal science. 2009;87(suppl_14):E101-E8.
37. Yan Y-E, Zhao Y-Q, Wang H, Fan M. Pathophysiological factors underlying heatstroke. Medical hypotheses. 2006;67(3):609-17.
38. Pearce S, Sanz-Fernandez M, Hollis J, Baumgard LH, Gabler NK. Short-term exposure to heat stress attenuates appetite and intestinal integrity in growing pigs. Journal of Animal Science. 2014;92(12):5444-54.
39. Manser CN, Kraus A, Frei T, Rogler G, Held L. The Impact of Cold Spells on the Incidence of Infectious Gastroenteritis and Relapse Rates of Inflammatory Bowel Disease: A Retrospective Controlled Observational Study. Inflammatory intestinal diseases. 2017;2(2):124-30.

40. Koh S-J, Kim JW, Kim BG, Lee KL, Kim JS. Restraint stress induces and exacerbates intestinal inflammation in interleukin-10 deficient mice. World Journal of Gastroenterology: WJG. 2015;21(28):8580.
41. Kayama H, Takeda K. Regulation of intestinal homeostasis by innate and adaptive immunity. International immunology. 2012;24(11):673-80.
42. Hayes MR, Mietlicki-Baase EG, Kanoski SE, De Jonghe BC. Incretins and amylin: neuroendocrine communication between the gut, pancreas, and brain in control of food intake and blood glucose. Annual review of nutrition. 2014;34:237-60.
43. Cox E, Schrauwen E, Cools V, Houvenaghel A. Experimental induction of diarrhoea in newly-weaned piglets. Journal of Veterinary Medicine Series A. 1991;38(1-10):418-26.
44. Arnal M-E, Lalles J-P. Gut epithelial inducible heat-shock proteins and their modulation by diet and the microbiota. Nutrition reviews. 2016;74(3):181-97.
45. Haque R, Roy S, Kabir M, Stroup SE, Mondal D, Houpt ER. Giardia assemblage A infection and diarrhea in Bangladesh. The Journal of infectious diseases. 2005;192(12):2171-3.
46. Hansson GC, Johansson ME. The inner of the two Muc2 mucin-dependent mucus layers in colon is devoid of bacteria. Gut microbes. 2010;1(1):51-4.
47. Alemu TW, Pandey HO, Wondim DS, Gebremedhn S, Neuhof C, Tholen E, et al. Oxidative and endoplasmic reticulum stress defense mechanisms of bovine granulosa cells exposed to heat stress. Theriogenology. 2018;110:130-41.
48. Pearce S, Mani V, Weber T, Rhoads R, Patience J, Baumgard L, et al. Heat stress and reduced plane of nutrition decreases intestinal integrity and function in pigs. Journal of Animal Science. 2013;91(11):5183-93.
49. Ishihara K, Hirano T. IL-6 in autoimmune disease and chronic inflammatory proliferative disease. Cytokine & growth factor reviews. 2002;13(4-5):357-68.
50. Kim J-A, Kim D-K, Tae J, Kang O-H, Choi Y-A, Choi S-C, et al. Acanthoic acid inhibits IL-8 production via MAPKs and NF-κB in a TNF-α-stimulated human intestinal epithelial cell line. Clinica chimica acta. 2004;342(1-2):193-202.
51. Kick AR, Tompkins MB, Almond GW. Stress and immunity in the pig. Animal Science Reviews. 2011;212:51-65.
52. Johansson ME, Hansson GC. Is the intestinal goblet cell a major immune cell? Cell host & microbe. 2014;15(3):251-2.
53. Bloemendaal AL, Buchs NC, George BD, Guy RJ. Intestinal stem cells and intestinal homeostasis in health and in inflammation: a review. Surgery. 2016;159(5):1237-48.
54. Li S, Tan H-Y, Wang N, Zhang Z-J, Lao L, Wong C-W, et al. The role of oxidative stress and antioxidants in liver diseases. International journal of molecular sciences. 2015;16(11):26087-124.
55. Albenberg L, Esipova TV, Judge CP, Bittinger K, Chen J, Laughlin A, et al. Correlation between intraluminal oxygen gradient and radial partitioning of intestinal microbiota. Gastroenterology.

2014;147(5):1055-63. e8.
56. Tian T, Wang Z, Zhang J. Pathomechanisms of oxidative stress in inflammatory bowel disease and potential antioxidant therapies. Oxidative medicine and cellular longevity. 2017;2017.
57. Handa O, Naito Y, Yoshikawa T. Helicobacter pylori: a ROS-inducing bacterial species in the stomach. Inflammation Research. 2010;59(12):997-1003.
58. Petrilli V. The multifaceted roles of inflammasome proteins in cancer. Current opinion in oncology. 2017;29(1):35-40.
59. Breitrück A, Sparmann G, Mitzner S, Kerkhoff C. Establishment of a novel extracorporeal bowel model to study luminal approaches to treat inflammatory bowel disease. Disease models & mechanisms. 2013;6(6):1487-93.
60. Reunanen J, Kainulainen V, Huuskonen L, Ottman N, Belzer C, Huhtinen H, et al. Akkermansia muciniphila adheres to enterocytes and strengthens the integrity of the epithelial cell layer. Appl Environ Microbiol. 2015;81(11):3655-62.
61. Diao H, Yan H, Xiao Y, Yu B, Yu J, He J, et al. Intestinal microbiota could transfer host Gut characteristics from pigs to mice. BMC microbiology. 2016;16(1):238.
62. Hill C. Balancing the risks and rewards of live biotherapeutics. Nature Reviews Gastroenterology & Hepatology. 2019:1-2.
63. Ng SC, Kamm MA, Yeoh YK, Chan PK, Zuo T, Tang W, et al. Scientific frontiers in faecal microbiota transplantation: joint document of Asia-Pacific Association of Gastroenterology (APAGE) and Asia-Pacific Society for Digestive Endoscopy (APSDE). Gut. 2020;69(1):83-91.
64. Nagao-Kitamoto H, Shreiner AB, Gillilland III MG, Kitamoto S, Ishii C, Hirayama A, et al. Functional characterization of inflammatory bowel disease–associated gut dysbiosis in gnotobiotic mice. Cellular and molecular gastroenterology and hepatology. 2016;2(4):468-81.
65. Lan A, Andriamihaja M, Blouin J-M, Liu X, Descatoire V, de Maredsous CD, et al. High-protein diet differently modifies intestinal goblet cell characteristics and mucosal cytokine expression in ileum and colon. The Journal of nutritional biochemistry. 2015;26(1):91-8.
66. Caporaso JG, Kuczynski J, Stombaugh J, Bittinger K, Bushman FD, Costello EK, et al. QIIME allows analysis of high-throughput community sequencing data. Nature methods. 2010;7(5):335.
67. Edgar RC. Search and clustering orders of magnitude faster than BLAST. Bioinformatics. 2010;26(19):2460-1.
68. Livak KJ, Schmittgen TD. Analysis of relative gene expression data using real-time quantitative PCR and the 2− ΔΔCT method. methods. 2001;25(4):402-8.
69. Rossi L, Vagni S, Polidori C, Alborali GL, Baldi A, Dell'Orto V. Experimental induction of Escherichia coli diarrhoea in weaned piglets. Open Journal of Veterinary Medicine. 2012;2(1):1-8.

Tables

Table 5. Diarrhea Index.#

Point	Degree of hardness/softness of feces
1	Hard, dry, and blocky
2	Hard
3	Soft
4	Soft
5	Watery
6	Watery, yellow, foamy

#Scored based on the method of Rossi et al.[69]

Table 6. Primer sequences.

Gene	Sequence (5′-3′)
IL-6	CACCGGTCTTGTGGAGTTTC
	GTGGTGGCTTTGTCTGGATT
IL-8	TTTCTGCAGCTCTCTGTGAGG
	CTGCTGTTGTTGTTGCTTCTC
IL-17	CCAGACGGCCCTCAGATTAC
	CACTTGGCCTCCCAGATCAC
β-actin	AAGTACTCCGTGTGGATCGG
	ACATCTGCTGGAAGGTGGAC

Figures

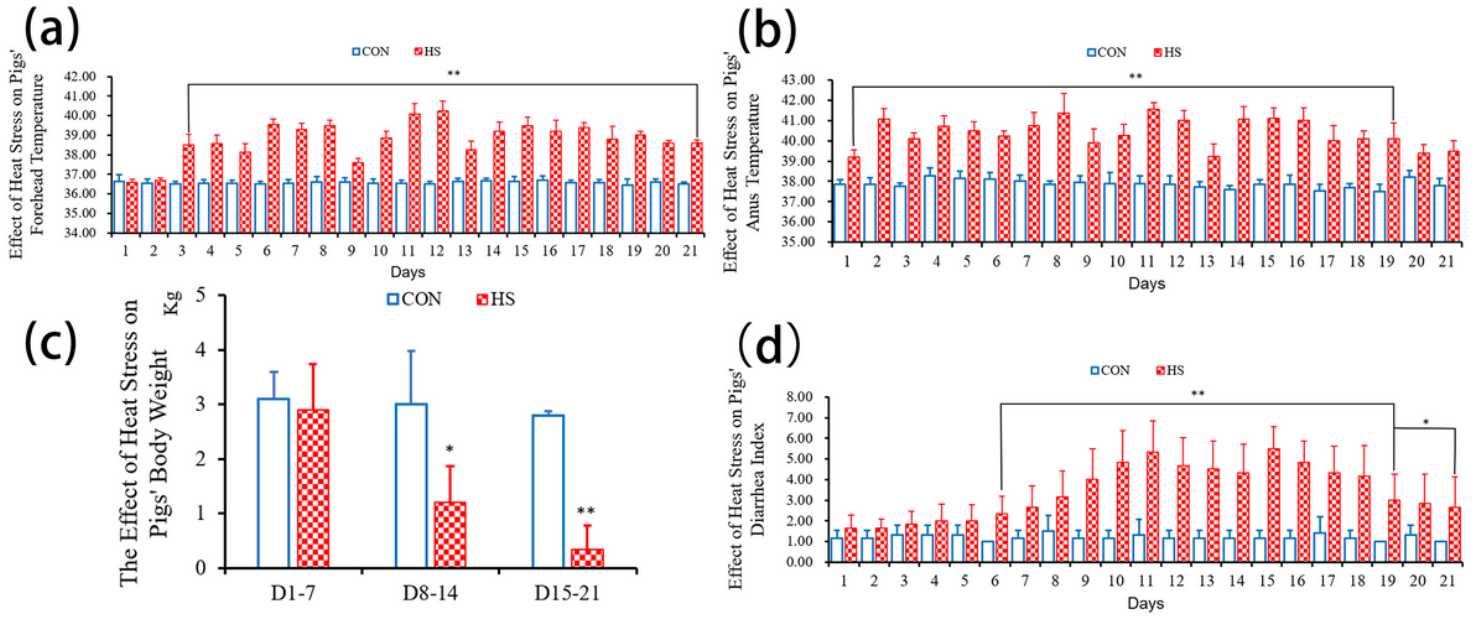

Figure 1

Effects of heat stress on pig growth performance. (a) forehead temperature, (b) rectal temperature, (c) body weight gain, (d) Diarrhea Index

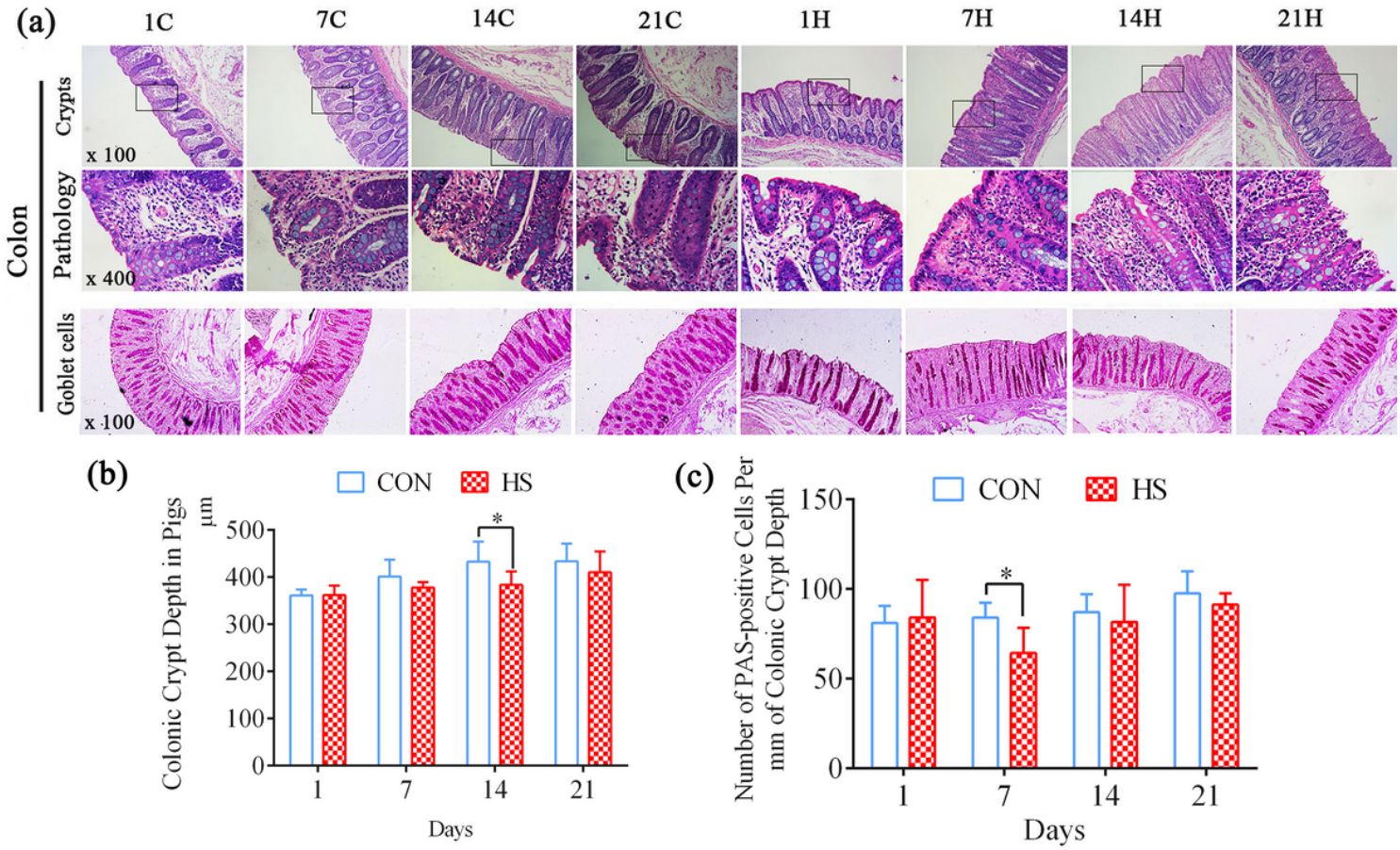

Figure 2

Effects of heat stress on colonic mucosal structure in pigs. Effects of heat stress on (a) crypt histopathology (H&E and PAS staining), (b) colon crypt depth (μm), and (c) number of PAS-positive cells per μm colon crypt depth. C and H refer to control- and heat-stressed pigs, respectively.

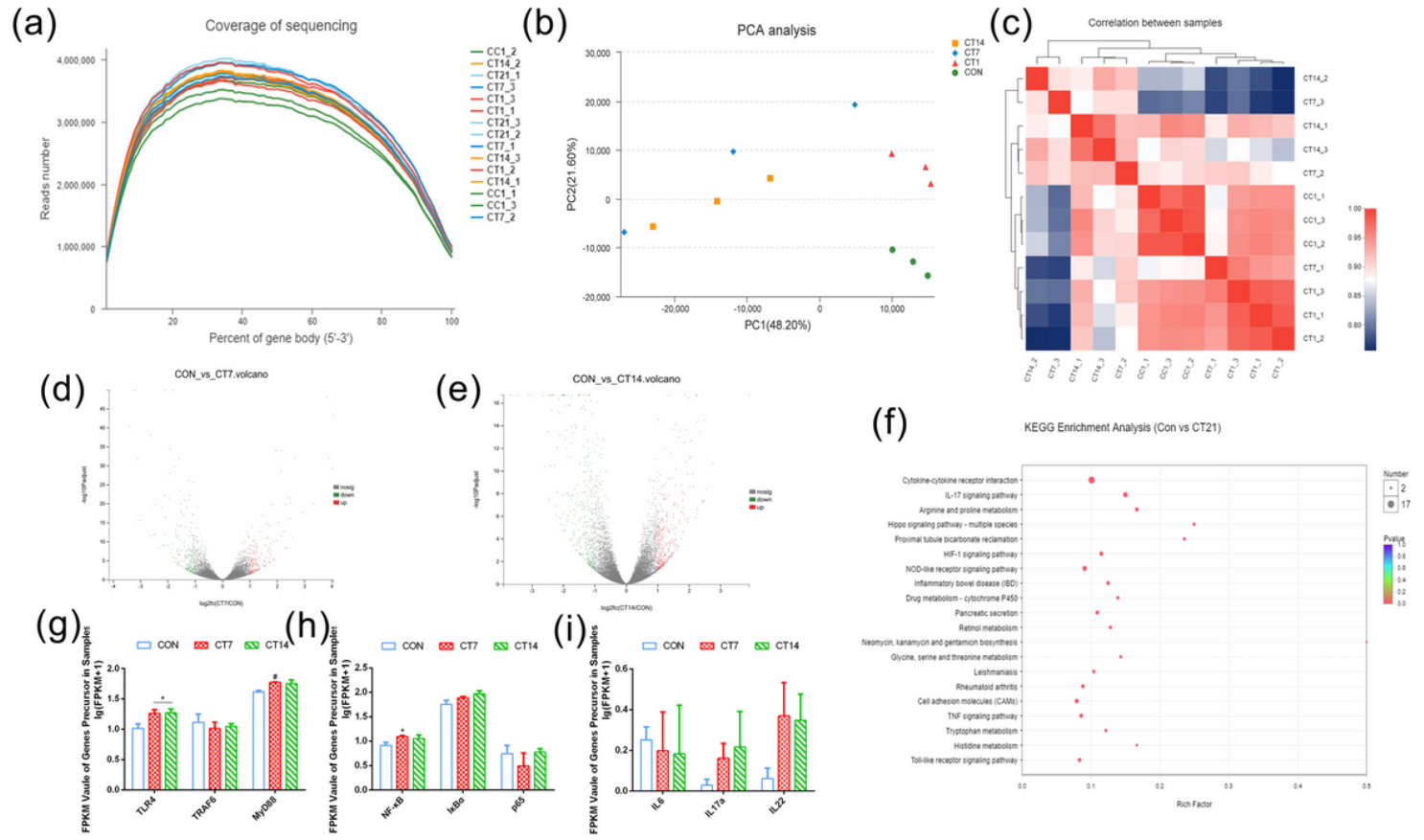

Figure 3

Effects of heat stress on pig colon transcriptomes. C/Con and T are control and heat stress, respectively; 1, 7, 14, and 21 are the days of heat treatment. (a) Gene coverage analysis (x-axis: 0 and 100 represent the 5'- and 3'-ends of the gene, respectively; y-axis: (reads number) sum of number of sequences in corresponding interval on horizontal axis position of all genes; (b) PCA of colonic epithelium; (c) heatmap analysis among samples; (d) differential expression volcanic plot (control vs. HS7); (e) differential expression volcanic plot (control vs. H14); (f) KEGG enrichment analysis (control vs. H7); (g)-(i) effects of heat stress on expression levels of key genes in TLR4/NF-κB signaling pathway.

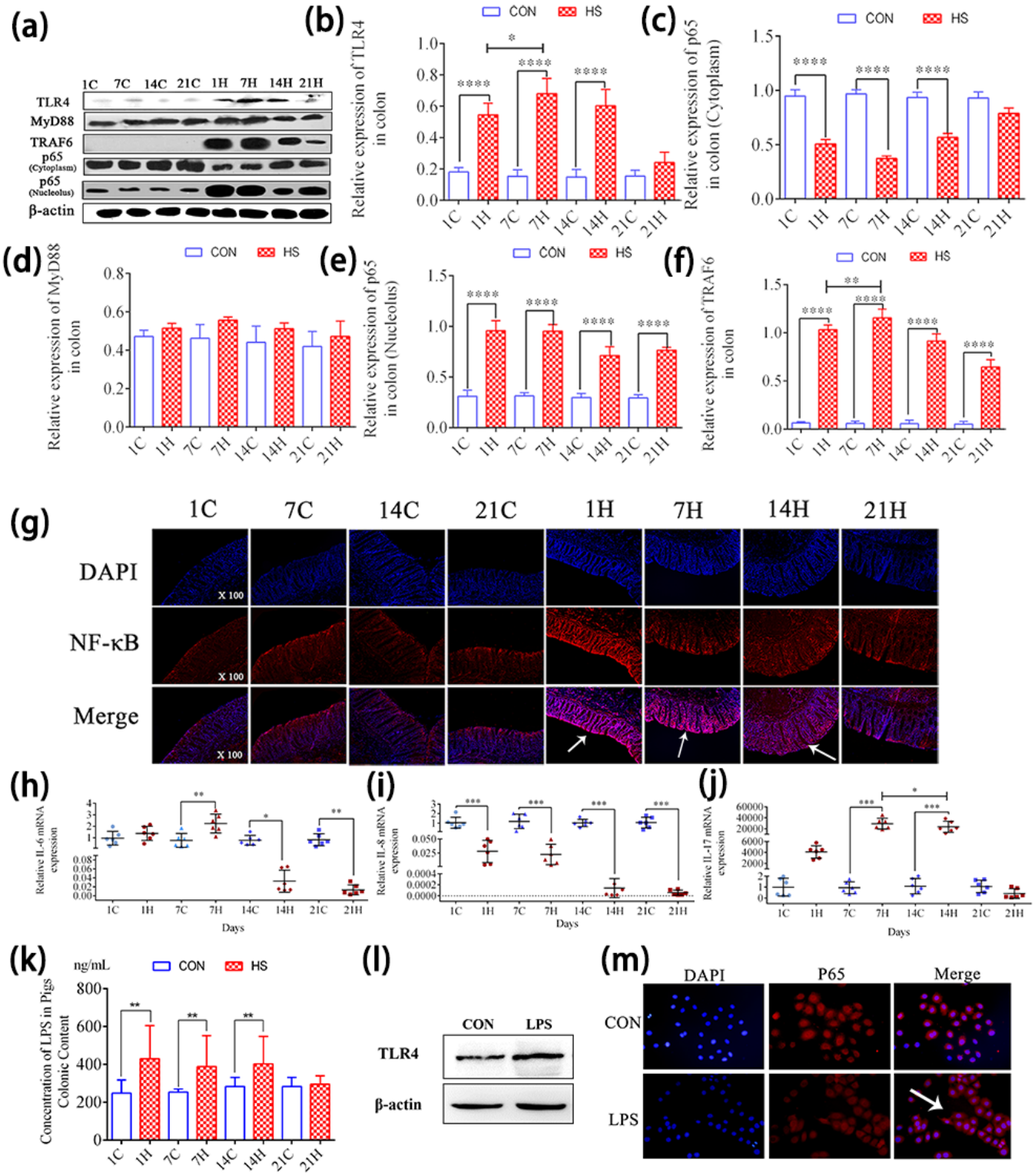

Figure 4

Expression of TLR4/NF-κB/p65 signaling pathway proteins in pig colon. (a) protein profiles; (b) TLR4; (c) p65 in cytoplasm; (d) MyD88; (e) p65 in nucleolus; (f) TRAF6; (g) p65-positive cell distribution in colonic mucosa (DAPI fluorescent nuclear dye); (h) IL-6 mRNA expression; (i) IL-8 mRNA expression; (j) IL-17 mRNA expression; (k) LPS concentration; (l) LPS induction of TLR4 in IPEC-J2; (m) p65-positive cell

distribution in IPEC-J2 (DAPI fluorescent nuclear dye). C and H refer to control- and heat-stressed pigs, respectively; 1, 7, 14, and 21 refer to sampling days.

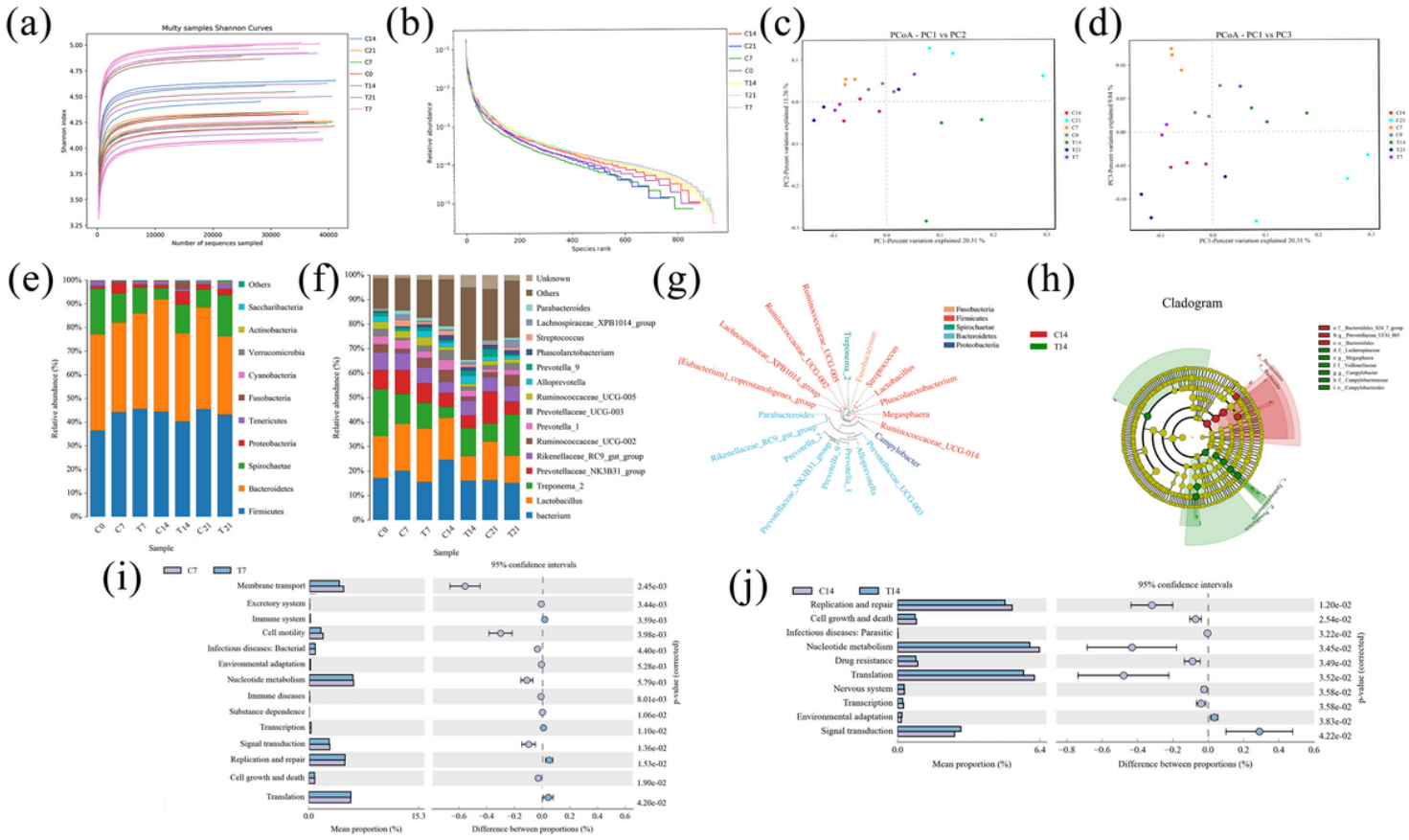

Figure 5

Effects of heat stress on pig feces microbiome. (a) Shannon index plot; (b) rank abundance curve; (c) & (d) PCA; (e) intestinal flora structure by phylum; (f) intestinal flora structure by genus; (g) phylogenetic tree analysis on day 14; (h) LEfSe analysis on day 14; (i) KEGG functional difference prediction (C7 vs. H7); (j) KEGG functional difference prediction (C14 vs. H14). C and H refer to control- and heat-stressed pigs, respectively; 1, 7, 14, and 21 refer to sampling days for pig feces and mouse transplantation.

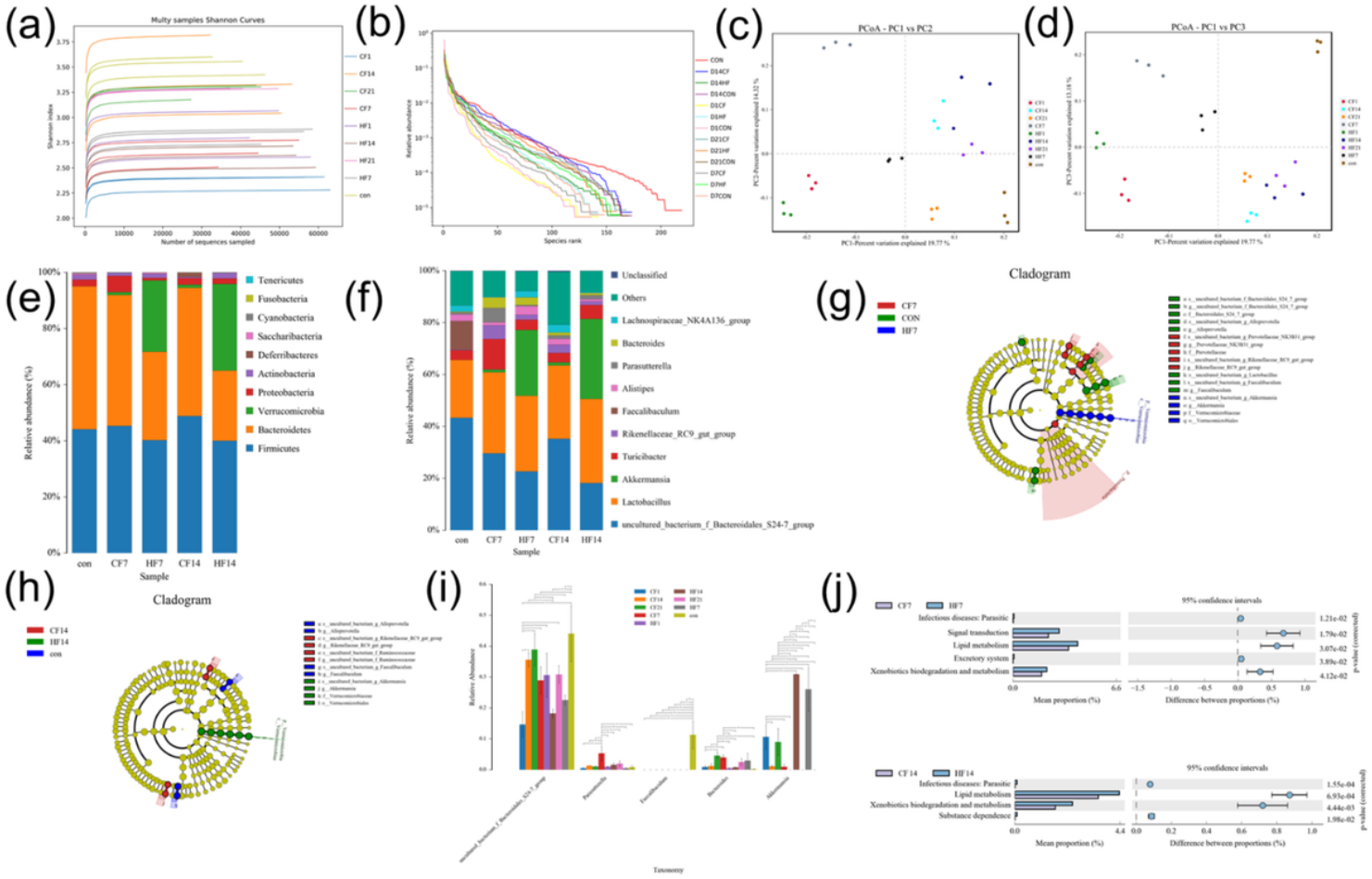

Figure 6

Effects of pig FMT on mouse colon microbiome. (a) Shannon index plot; (b) rank abundance curve; (c) & (d) PCA; (e) intestinal flora structure by phylum; (f) intestinal flora structure by genus; (g) LEfSe analysis between CF7 and HF7; (h) LEfSe analysis between CF14 and HF14; (i) ANOVA of genera; (j) KEGG functional difference prediction (CF7 vs. HF7; CF14 vs. HF14). CF & HF refer to infusion with feces from control- and heat-stressed animals, respectively; 1, 7, 14, and 21 refer to sampling days of pig feces and mouse transplantation.

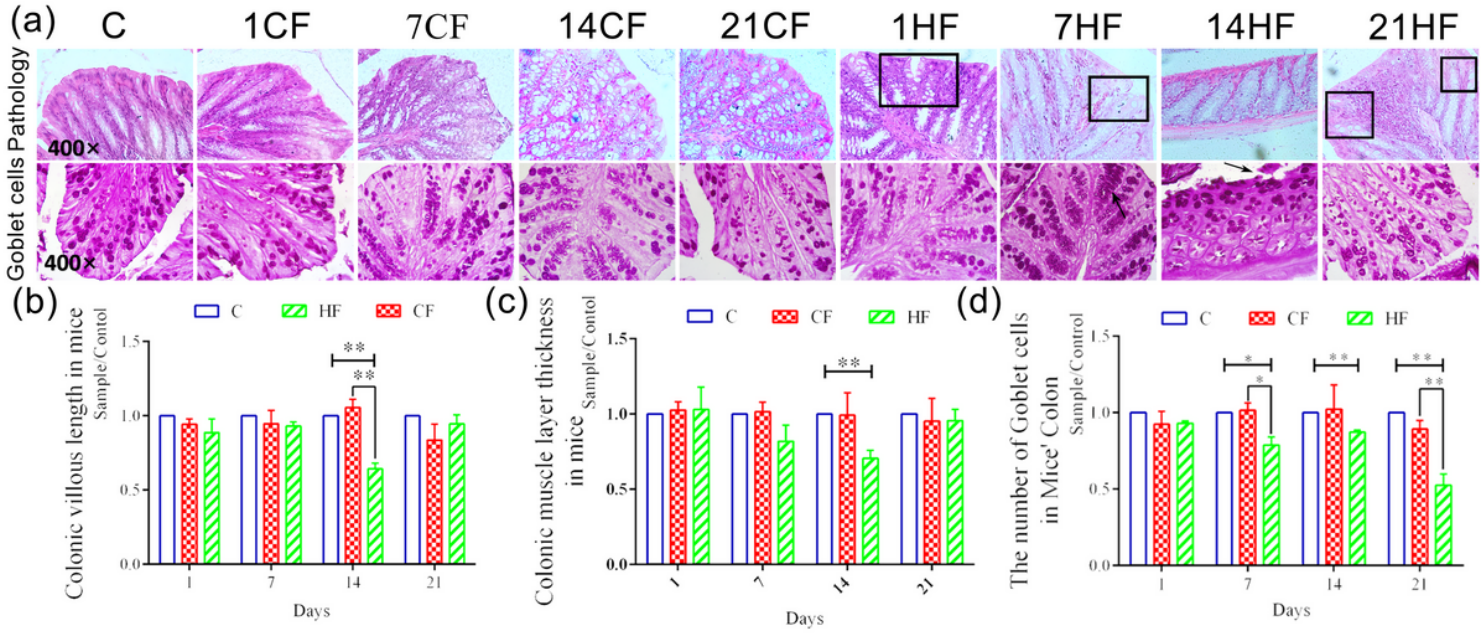

Figure 7

Effects of pig FMT on histopathology of mouse colonic mucosa. (a) H&E and PAS staining; (b) colon villus length; (b) colon muscle layer thickness; (d) number of PAS-positive goblet cells per mm2 colonic mucosa. CF & HF refer to infusion with feces from control-– and heat-stressed animals, respectively; 1, 7, 14, and 21 refer to sampling days of pig feces and mouse transplantation.

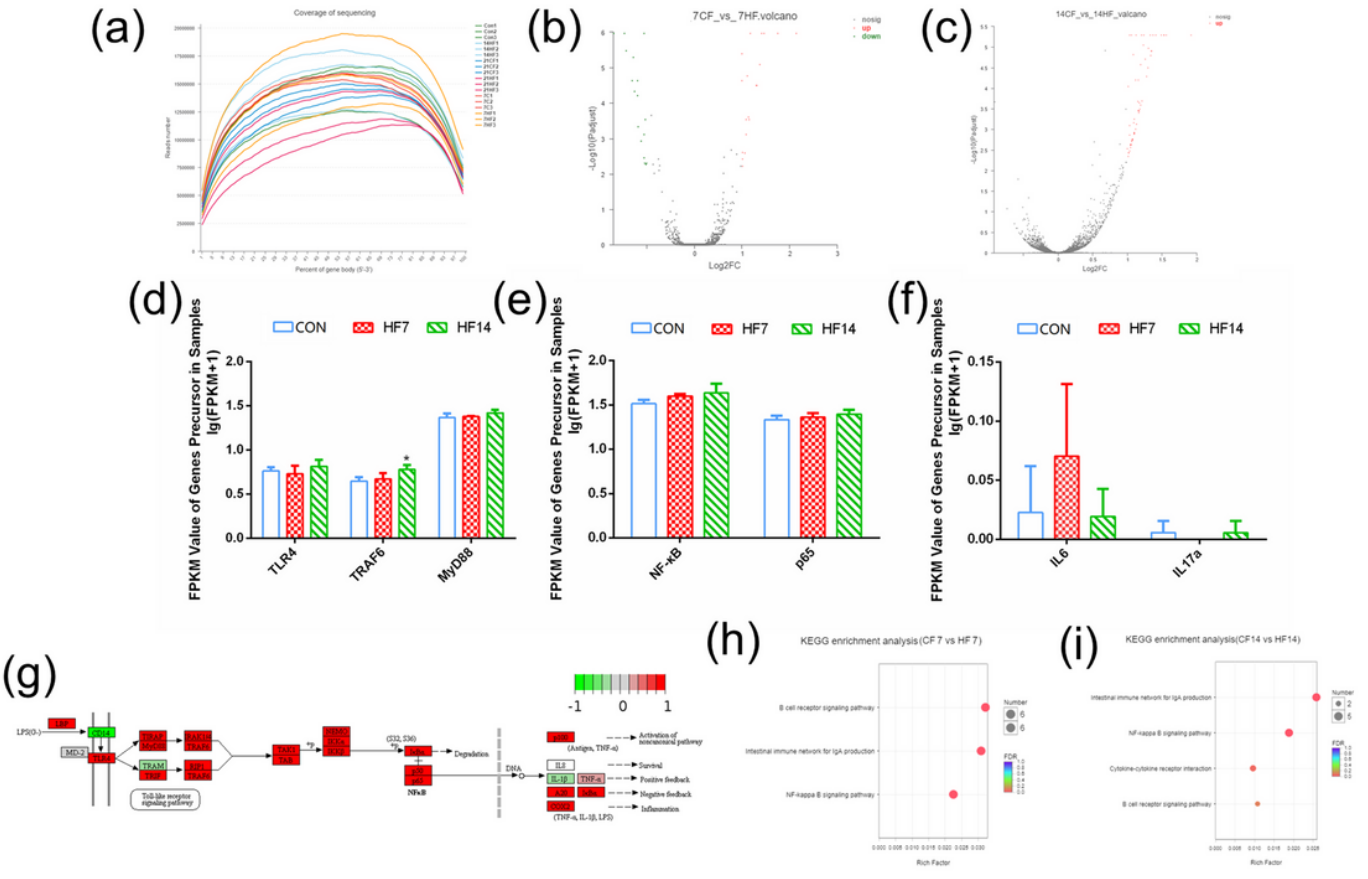

Figure 8

Effects of pig FMT on TLR4/NF-KB signaling pathway expression in mouse colon (transcriptomics). (a) gene coverage analysis; on abscissa, 0 and 100 represent 5'- and 3'-end of gene, respectively; ordinate is sum of number of sequences in corresponding interval on horizontal axis position of all genes; (b) differential expression volcanic plot (CF7 vs. HF7); (c) differential expression volcanic plot (CF14 vs. HF14); (d)-(f) FPKM for TLR4, TRAF6, MyD88, NF-κB, p65, IL6, and IL17α precursors; (g) expression level of TLR4/NF-κB signaling pathway in HF14; (h) KEGG enrichment analysis (CF7 vs. HF7); (i) KEGG enrichment analysis (CF14 vs. HF14).

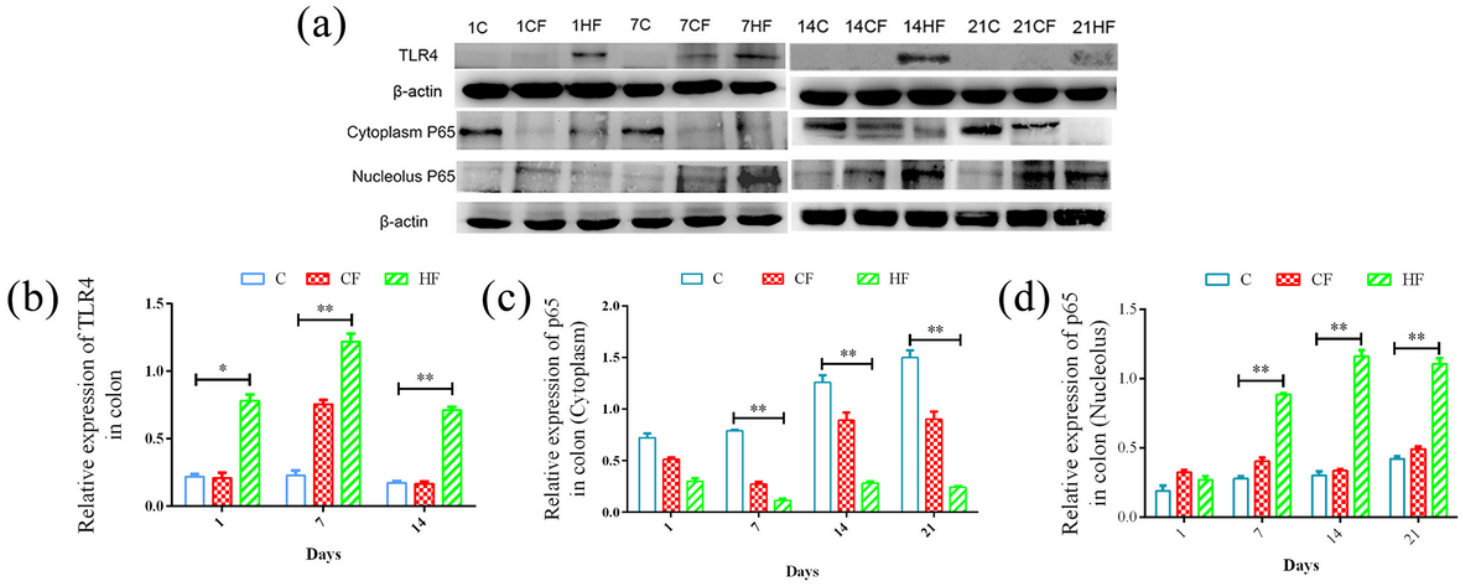

Figure 9

Expression of key proteins in TLR4/NF-κB/p65 signaling pathway in mouse colon 1 wk after FMT. (a) Western blot of TLR4/NF-κB signaling pathway in colon; (b) heat stress response of TLR4; (c) heat stress response of nuclear p65; (d) heat stress response of cytoplasmic p65. C, CF, and HF are control mice, mice infused with control-group pig feces, and mice infused with heat-stressed-group pig feces, respectively; 1, 7, 14, and 21 refer to sampling days of pig feces and mouse transplantation.